JOURNAL OF GUIDANCE, CONTROL, AND DYNAMICS
Vol. 32, No. 1, January–February 2009

Quantized Control Allocation of Reaction Control Jets and Aerodynamic Control Surfaces

David B. Doman,* Brian J. Gamble,† and Anhtuan D. Ngo‡
U.S. Air Force Research Laboratory, Wright–Patterson Air Force Base, Ohio 45433-7531

DOI: 10.2514/1.37312

A mixed-integer linear programming approach to mixing continuous and pulsed control effectors is proposed. The method is aimed at applications involving reentry vehicles that are transitioning from exoatmospheric flight to endoatmospheric flight. In this flight phase, aerodynamic surfaces are weak and easily saturated, and vehicles typically rely on pulsed reaction control jets for attitude control. Control laws for these jets have historically been designed using single-axis phase-plane analysis, which has proven to be sufficient for many applications where multi-axis coupling is insignificant and when failures have not been encountered. Here, we propose using a mixed-integer linear programming technique to blend continuous control effectors and pulsed jets to generate moments commanded by linear or nonlinear control laws. When coupled with fault detection and isolation logic, the control effectors can be reconfigured to minimize the impact of control effector failures or damage. When the continuous effectors can provide the desired moments, standard linear programming methods can be used to mix the effectors; however, when the pulsed effectors must be used to augment the aerodynamic surfaces, mixed-integer linear programming techniques are used to determine the optimal combination of jets to fire. The reaction jet control allocator acts as a nonuniform quantizer that applies a moment vector to the vehicle, which approximates the desired moment generated by a continuous control law. Lyapunov theory is applied to develop a method for determining the region of attraction associated with a quantized vehicle attitude control system.

I. Introduction

REACTION control systems (RCS) that consist of thrusters that can fire to produce rolling, pitching, and yawing moments have been used for entry vehicle control for decades. In exoatmospheric flight, entry vehicles may be entirely dependent upon such systems for attitude control. As a vehicle enters the atmosphere, aerodynamic forces and moments begin to act on the vehicle, which can either stabilize or destabilize the body. Also, on vehicles equipped with aerodynamic control surfaces, additional attitude control devices gain control power as dynamic pressure increases as the vehicle transitions from exoatmospheric to endoatmospheric flight. RCS jets can be characterized as pulsed unilateral control effectors with two states (off/on). Aerodynamic surfaces are rate and position limited; however, they can produce a continuum of forces and moments when operating within these limits. Methods for blending pulsed RCS and continuously variable control surfaces are proposed.

Historically, single-axis phase-plane analysis has been a powerful and effective tool for designing control laws for entry vehicles, such as the Apollo command module [1] and the Mars Science Laboratory [2]. The shuttle RCS system was derived from the Apollo and Skylab programs; however, because the shuttle has only one plane of symmetry, rotational coupling problems led to numerous changes [3,4]. The design of the X-33 ultimately incorporated 10 RCS jets into the vehicle design, which were placed in such a way that resulted in significant rotational coupling between the roll, pitch, and yaw axes [5].

An alternative to the phase-plane methods for control of such vehicles was proposed by Paradiso [6], who developed a linear programming (LP) based approach to blending aerodynamic surfaces with RCS jets. The method treated the RCS jets as continuous effectors by using pulse width modulation (PWM) to vary the jet duty cycle. An advantage of such an approach is that continuous multivariable control methods may be applied to the control design problem, allowing more sophisticated and efficient design techniques to be applied to a system with continuous and pulsed control effectors. The method was also capable of fault-tolerant operation when coupled with fault-detection logic, because the control mixing was designed to be performed in real time. PWM methods may, however, lead to rapid cycling of the jets, which can result in excessive wear on the RCS propellant control valves. Although not an issue for expendable launch vehicles, this wear can create maintenance issues on reusable systems. The PWM method, as will be seen in a comparison with the proposed method of this paper, was found to use less propellant when regulating attitude around low-amplitude terminal limit cycles near zero error, but at the expense of higher jet cycling. In addition, there are practical limits to PWM duty cycles for RCS systems, for example, shuttle RCS thrusters have an 80 ms cycle-time granularity [4].

Here, we propose a mixed-integer linear programming (MILP) formulation of the RCS mixing problem that is designed to be daisy-chained with a standard LP solution to the aerosurface control allocation problem. That is, the RCS control allocator is designed to operate when the aerosurfaces have saturated and are unable to supply the moment vector commanded by an attitude control system. The RCS allocator is designed to deliver the residual desired moment vector as closely as possible (in a 1-norm sense) without any element of the RCS torque vector exceeding the magnitude of any element of the RCS torque command vector. The RCS control allocator thus acts as a quantization element that translates continuous torque command vectors in $\mathbb{R}^3$ into quantized torque vectors in $\mathbb{R}^3$ that meet the previously described optimization criteria. Treating the RCS control allocator as a quantization element is advantageous in light of recent developments in stability analysis for quantized control systems [7–9]. The advantage of using a quantized control approach is that multivariable control methods may be used to design tracking and

Presented as Paper 6778 at the AIAA Guidance, Navigation and Control Conference and Exhibit, Hilton Head, SC, 20–23 August 2007; received 26 February 2008; revision received 30 April 2008; accepted for publication 6 May 2008.

*Senior Aerospace Engineer, Control Design and Analysis Branch, 2210 Eighth Street, Suite 21; David.Doman@wpafb.af.mil. Associate Fellow AIAA.

†Captain, U.S. Air Force, Aerospace Engineer, Control Design and Analysis Branch, 2210 Eighth Street, Suite 21; Brian.Gamble@wpafb.af.mil.

‡Electronics Engineer, Control Design and Analysis Branch, 2210 Eighth Street, Suite 21; anhtuan.ngo@wpafb.af.mil.

stability augmentation systems for situations where multi-axis coupling exists and phase-plane design methods become intractable. In principle, control laws can be designed using any convenient method and the RCS control allocator can be used to deliver a quantized approximation of the desired torque vector generated by a continuous control law. Although the examples in this paper represent quantized approximations of linear control laws, the method is equally well suited for use with nonlinear control laws. When used in conjunction with a fault detection and isolation (FDI) system, the control allocator can be used to reconfigure the system to minimize the impact of failures. It is important to note that failures and reconfiguration may change the quantization behavior of the allocators and may therefore also affect closed-loop stability. Lyapunov theory is applied to determine the region of attraction for a quantized feedback control law acting on a linear time-invariant plant.

II. Reaction Control System Modeling

RCS thrusters are fundamentally force-producing devices that are controlled by valves that turn the thrusters on and off. Ideally, each thruster instantaneously produces a force vector $\mathbf{F} = F\hat{\mathbf{n}}$ when a fire command is issued, where F is the magnitude of the thrust and $\hat{\mathbf{n}}$ is a unit vector in the direction of the thrust. Each thruster is located at a distance $\mathbf{r}$ from the vehicle center of gravity for the purpose of producing a torque vector $\boldsymbol{\tau} = \mathbf{r} \times \mathbf{F}$ when aerodynamic forces and moments produced by conventional surfaces are weak when operating at low dynamic pressures. Multiple jets may be fired to approximate a desired torque command but, because the jets are switched devices, only 2^p distinct torques can be achieved, where p is the number of jets.

It is important to note that there are a number of practical issues that this ideal model does not capture. The forces produced by real RCS jets are not constant. When a command to fire is received, the force ramps up to a steady-state value over a finite time and, conversely, the force takes some time to ramp down to zero when the fire command is removed. This implies that some minimum duty cycle time exists for a particular RCS implementation. Also, multiple RCS jets may draw propellant from one reservoir, which may not have the capacity to simultaneously supply all jets with propellant at constant pressure. The implication is that, as the number of active jets increases, the less force each thruster will produce. Also, thruster performance can decrease as the propellant reservoir pressure decreases as the quantity of propellant decreases. Furthermore, jet performance will change as a function of atmospheric pressure, as the vehicle enters into the atmosphere as a result of over/under expanded flow through the nozzle.

III. Formulation for Reaction Control System Thruster Allocation

Standard linear-programming-based control allocation methods can be used to solve for the aerodynamic surface positions that satisfy moment commands from a control law when these commands are physically realizable. In the event that these continuously variable effectors are incapable of delivering the required moment in one or more axes, axis saturation is said to occur. If a suite of RCS jets are available to compensate for the lack of continuous control power, these jets may be fired to augment the continuously variable control effectors with quantized feedback control moments generated by the RCS, which approximate the moment commands from a continuous control law. Because of the discrete state nature of the RCS jets, the exact moment demands will only be met when the sum of the continuous and discrete state effector moments are coincident with the moment demand. Furthermore, it is undesirable to fire the jets in such a way as to cause the continuous control effectors be commanded to move instantaneously from one position to another in an effort to drive the moment error to zero, because such logic will likely cause the continuous surfaces to chatter and rate limit. Thus, we propose to use integer linear programming and linear programming techniques to implement a quantization strategy that allows a controller to close the loop using a control allocator, which minimizes the difference between the moment demands and the actual moments delivered, subject to the resolution limits imposed by the RCS.

Numerous control allocation methods exist that allow one to blend control effectors whose positions can be continuously varied to achieve a desired torque command, subject to rate and position limits. For a more comprehensive look into the many control allocation methods available for continuously variable control effectors, the reader is referred to the following survey and tutorial papers on the subject [10–13]. Most methods employ optimization techniques to solve problems of the form

$$\min_{\boldsymbol{\delta}} \sum_{j=1}^{n} g_i(\delta_j) = d_{i_{\text{des}}}, \qquad i = 1, \ldots, 3 \tag{1}$$

subject to

$$\boldsymbol{\delta}_{\min} \le \boldsymbol{\delta} \le \boldsymbol{\delta}_{\max} \qquad \dot{\boldsymbol{\delta}}_{\min} \le \dot{\boldsymbol{\delta}} \le \dot{\boldsymbol{\delta}}_{\max} \tag{2}$$

where $g_i(\delta_j)$ are functions relating control effector positions to the torques produced by those effectors, and $d_{i_{\text{des}}}$ are the desired control induced torques that are usually specified by a control law. Note that we are concerned with a three-moment problem where we are interested in producing pitching, rolling, and yawing moments, thus $i = 1, \ldots, 3$. In most approaches, $g_i(\delta_j)$ must be linear functions; however, a technique called piecewise linear control allocation has been developed that handles situations where the torques produced by the effectors are nonlinear but separable functions of control surface positions [12].

Continuous control allocation problems may be solved by any convenient method [10,11] to blend aerodynamic control effectors in the atmosphere. For RCS-equipped vehicles in exoatmospheric flight, the vehicle must be controlled using these pulsed effectors. In flight through the upper atmosphere, a blend of RCS and continuously variable aerodynamic effectors may be necessary. We begin by developing some formulations for the former case, which will later be combined with standard LP-based control allocation techniques to create a control allocation strategy for the latter.

A. Formulation for Reaction Jet Allocation in Exoatmospheric Flight

In exoatmospheric flight, just before entry, a vehicle may be required to use only the RCS jets to regulate attitude. Historically, many vehicles have been designed with RCS systems where each jet is positioned such that its primary effect is upon a single axis (i.e., roll, pitch, or yaw). Control mixing for such designs is often done using simple jet ganging, whereas the control laws use single-axis phase-plane design techniques. More recently, some reusable launch vehicle designs have incorporated reaction control jets that have significant effects upon more than one axis, making the problem of jet blending less straightforward. Furthermore, the implementation of fault-tolerant integrated adaptive guidance and control systems [14] require online reconfiguration of the control effectors in the event of one or more failures, making a fixed ganging approach to control allocation incapable of maintaining vehicle control, even though sufficient control power may exist.

The proposed primary control allocation objective is to minimize the difference between the desired torque components and those produced by the RCS jets, whereas the secondary objective is to minimize propellant usage. The solution is also subject to the constraint that the magnitude of the torque produced by the RCS jets in each axis does not exceed the desired torque command. Thus, we propose the following formulation of the pulsed control effector control allocation problem:

$$\min_{\mathbf{u}} \sum_{i=1}^{3} w_{\text{axis}_i} |\tau_{i_{\text{des}}} - \sum_{k=1}^{p} T_{i,k} u_k| + \sum_{k=1}^{p} w_k u_k \tag{3}$$

subject to

$$0 \le \sum_{k=1}^{p} T_{i,k} u_k \le \tau_{i_{\text{des}}} \quad \forall\ \tau_{i_{\text{des}}} \ge 0$$
$$0 \ge \sum_{k=1}^{p} T_{i,k} u_k \ge \tau_{i_{\text{des}}} \quad \forall\ \tau_{i_{\text{des}}} < 0 \tag{4}$$

where w_{axis_i} are weights that allow one to vary the penalty on errors in the roll, pitch, and yaw axes, $w_k \ge 0$ are weights that allow one to vary the penalty associated with firing the kth jet, and u_k is a binary number (i.e., zero or one) that represents the state of the kth RCS thruster (on or off). $T_{i,j}$ represents the torque produced by the jth thruster on the ith axis when fired, and $\tau_{i_{\text{des}}}$ is the desired total thruster torque in the ith axis, where $i = 1, \ldots, 3$ (i.e., roll, pitch, and yaw axes). The constraint given by Eq. (4) defines the quantization strategy. One could, in principle, choose any quantization strategy; however, here, we choose a condition that is designed to be conservative when used in conjunction with a continuous feedback control law that operates on an open-loop stable system. Note that this constraint ensures that the effective torque commands never exceed the magnitude of the torques commanded by the continuous control law. This quantization strategy is designed to avoid inadvertently increasing the effective gains of a continuous controller. Also note that torque quantization in the case of RCS actuation is not necessarily applied in uniform increments, which is in contrast to quantization commonly encountered in sensor measurements.

In principle, for any desired torque vector $\boldsymbol{\tau}_{\text{des}}$, a global minimum can be found by searching over 2^p combinations of thruster firings and selecting the configuration with the smallest error that satisfies the constraint given by Eq. (4). For small p, this may be the best approach to solving the thruster firing problem, because convergence can be guaranteed in a finite number of steps. If in the worst case, the time it takes to execute those steps on a flight computer lies within the time frame allocated for the determination of a thruster firing solution, then this direct approach may be desirable. If not, then more efficient solution methods may be employed; however, these may come with a lack of convergence guarantees or could, in the worst case, require cycling through 2^p combinations to determine a solution. An upper bound on the number and type of computations required to arrive at a solution by enumeration is given in Table 1. Note that certain terms, for example,

$$\sum_{k=1}^{p} w_k u_k$$

and

$$\sum_{k=1}^{p} T_{i,k} u_k$$

in Eqs. (3) and (4), can be evaluated offline and stored in tables because they do not change in exoatmospheric flight. The storage of these terms results in a savings of $(p-1)2^{p+2}$ addition operations and $p2^{p+2}$ multiplication operations per flight control time step. In endoatmospheric flight, the elements of the torque matrix may be a function of flight condition, and the multiplication and addition operations may have to be performed; however, the multiplications are trivial in the sense that they consist of torque matrix elements multiplied by zero or one. These bounds may be used to calculate the maximum computation time required to solve the quantized control allocation problem by enumeration for any selected processor, compiler, and level of floating point precision.

Table 1 Number of operations required at each flight control system update to solve quantized control allocation problem by enumeration

Operation	Number
Multiplications	$3(2^p)$
Additions	$6(2^p)$
Comparisons	$9(2^p)$

B. One-Degree-of-Freedom Example

To motivate and elucidate the preceding formulation, a 1-degree-of-freedom example is shown because the quantized control of such systems can be visualized in the phase plane.

Consider a frictionless disk with a polar moment of inertia J that is free to rotate about its center. From Newton's law

$$\tau = J\ddot{x} \tag{5}$$

where x is the angular position and τ is an external torque. If a suitable actuator and sensor suite were available, one could implement a continuous time control law to achieve a damped second-order closed-loop response to regulate the angular position to zero by proper selection of τ:

$$\tau = J(-2\zeta\omega_n \dot{x} - \omega_n^2 x) \tag{6}$$

where ζ is the desired closed-loop damping ratio and ω_n is the desired closed-loop natural frequency. In the example shown in Fig. 1, we consider a case where four pulsed thrusters are available for control. We wish to use these thrusters to provide a quantized approximation of the continuous control law defined by Eq. (6). Each thruster is located 1 unit from the center. Two thrusters produce 1 unit of force, whereas the other two produce 2 units of force. For simplicity, the moment of inertia of the disk is taken to be unity. In the phase plane, torque commands generated by the linear continuous control law of Eq. (6) map into an infinite number of lines of constant torque. Thus, the linear control law of Eq. (6) has infinite resolution in the phase plane because it implicitly assumes that any torque can be achieved. For the case of the aforementioned discrete thruster arrangement, there are 16 possible combinations of jet firings; however, there are only seven distinct torques that can be achieved, namely, $(0, \pm 1, \pm 2, \pm 3)$. When implementing the proposed quantization approach to this special case, the phase plane gets divided into seven regions, each of which is associated with one of the seven distinct torques that the thrusters can generate. Figure 2 shows these seven regions that are bounded by specific lines of constant torque, which are a subset of the lines of constant torque associated with the continuous controller. Using this approach to quantization, the thrusters only produce the exact torque requested by the continuous control law when the state trajectory passes through one of the seven

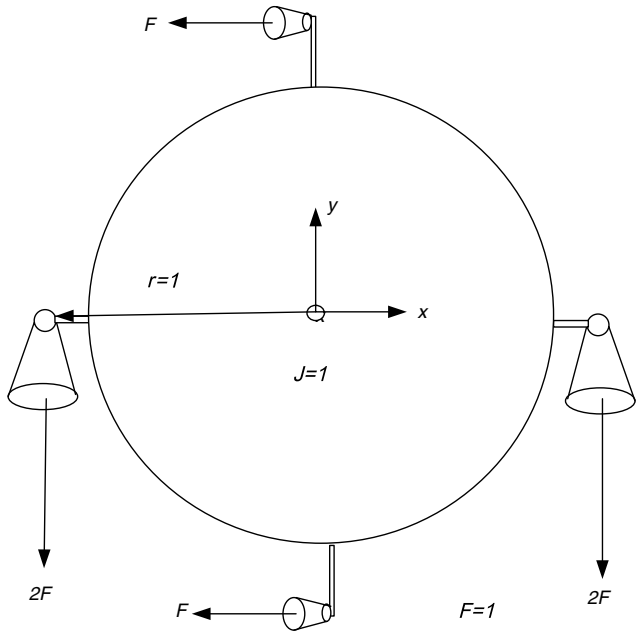

Fig. 1 One-degree-of-freedom frictionless disk with four thrusters.

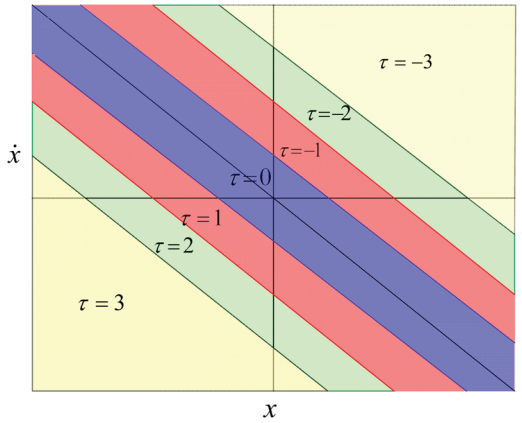

Fig. 2 Quantized controller torque mapping in phase plane for a 1-degree-of-freedom frictionless disk with four thrusters.

lines of constant torque where the continuous controller and the quantized controller coincide, otherwise, the quantized controller always rounds down toward the next smallest torque achievable by the thruster suite. As mentioned earlier, the choice of quantization strategy is designed to avoid having the quantized control law produce larger effective gains than the continuous control law at all points in the phase space. Finally, note that, because there are only seven distinct torques achievable from 16 possible thruster firing combinations, the question of solution uniqueness arises. The most obvious example being the case in which there are four thruster firing solutions that achieve $\tau = 0$, namely, fire no jets, fire ± 1, fire ± 2, or fire ± 1 and ± 2. Obviously, one would choose to fire no jets to achieve $\tau = 0$, if propellant conservation were a concern. This is ensured by the use of the second summation term in Eq. (3), which penalizes the use of thrusters and thereby guides the solution toward thruster combinations that minimize propellant usage, while meeting the torque demands as closely as possible without exceeding them. The penalty on control usage reduces the solution space; however, it does not completely solve the issue of multiple solutions. If solution uniqueness is a concern, additional terms, such as penalties on switch transitions, can be added to ensure that a unique solution does exist. Figure 3 shows an initial condition response from the state $\dot{x}(0) = 1$ rad/s, $x(0) = 1.2$ rad under quantized RCS control. The continuous control command is the desired value of torque at any instant, with $\zeta = 0.7$, $\omega = 3$. Note that the quantized control input is always less than or equal to the continuous command when the continuous command is positive. When the continuous command is negative, the quantized control input is always greater than or equal to the continuous command, per Eq. (4). The phase trajectories of Eq. (5), resulting from the application of constant nonzero torques, can be shown to be a family of parabolas. The offsets and shapes of these parabolas are governed by the initial condition and the magnitude of the torque. Figure 4 shows the phase trajectory of the initial condition response under quantized feedback for the previously considered case. Note that the parabolic shapes change as the system crosses quantization zones in the phase plane, except in coast phases, where they take the form of a line of zero slope as the system passes through the zero-torque dead zone.

Although it is instructive to observe the behavior of the proposed quantization strategy in the phase plane, the practical utility of the method lies in its ability to systematically control multi-axis coupled systems with pulsed thrusters.

C. Mixed-Integer Linear Programming Formulation

We will now present a MILP formulation for the pulsed effector control allocation problem. This will allow one to make use of one of the many solvers that are available for the solution of such problems. First, we define a vector of slack variables:

$$\mathbf{u}_s \triangleq \boldsymbol{\tau}_{\text{des}} - \mathbf{T}\mathbf{u} \tag{7}$$

where $\boldsymbol{\tau} \in \mathbb{R}^3$ is the desired torque vector, $\mathbf{T} \in \mathbb{R}^{3\times \mathbf{p}}$ is a matrix whose columns represent the body-axis torque vector that can be produced by each thruster when fired, and $\mathbf{u}$ is a vector of binary numbers where each element represents the (on/off) state of each thruster. Note that $\mathbf{u}_s \in \mathbb{R}^{\mathbf{3}}$, and $\mathbf{u}$ is a vector of binary variables, which together form the decision variables for the following MILP that will produce a solution to the optimization problem posed in Eq. (3):

$$\min_{\mathbf{u},\mathbf{u}_s} \begin{bmatrix} w_1 & w_2 & \dots & w_p \end{bmatrix} \begin{bmatrix} w_{\text{roll}} & w_{\text{pitch}} & w_{\text{yaw}} \end{bmatrix} \begin{bmatrix} \mathbf{u} \\ \mathbf{u}_s \end{bmatrix} \tag{8}$$

subject to

$$\begin{bmatrix} -\mathbf{u}_s \\ \mathbf{T}\mathbf{u} - \mathbf{u}_s \\ -\mathbf{T}\mathbf{u} - \mathbf{u}_s \end{bmatrix} \leq \begin{bmatrix} \mathbf{0} \\ \boldsymbol{\tau}_{\text{des}} \\ -\boldsymbol{\tau}_{\text{des}} \end{bmatrix}$$

and

$$0 \leq \sum_{k=1}^{p} T_{i,k} u_k \leq \tau_{i_{\text{des}}} \quad \forall\ \tau_{i\text{des}} \geq 0$$

$$0 \leq -\sum_{k=1}^{p} T_{i,k} u_k \leq -\tau_{i_{\text{des}}} \quad \forall\ \tau_{i_{\text{des}}} < 0$$

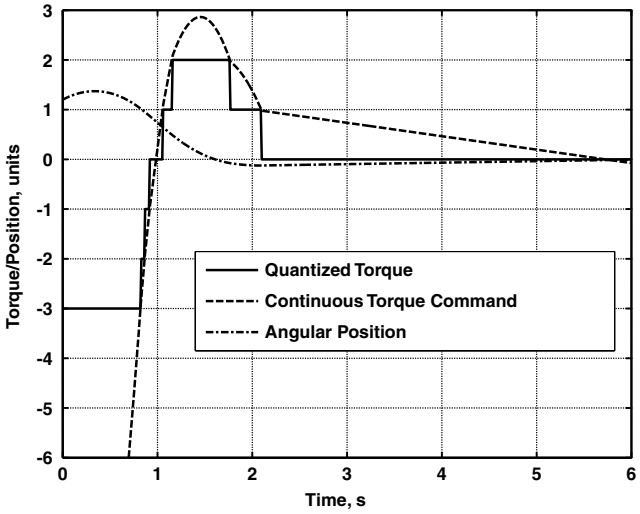

Fig. 3 Quantized control time history of 1-degree-of-freedom frictionless disk.

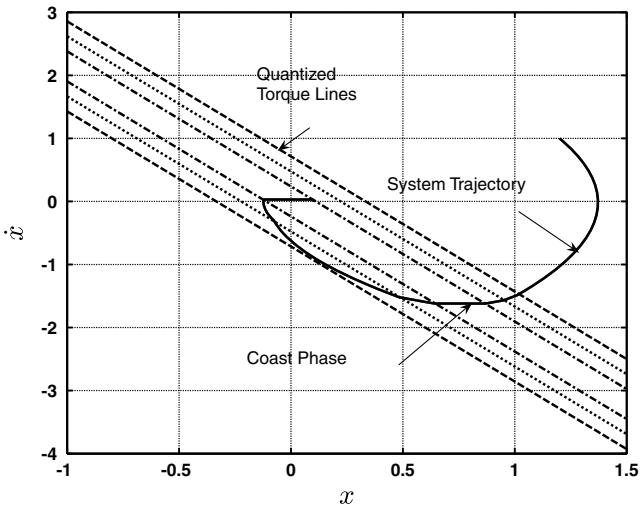

Fig. 4 Initial condition response of 1-degree-of-freedom frictionless disk in the phase plane.

The MILP formulation provides the convenience of using off-the-shelf solvers to solve the quantized control allocation problem; however, the upper bound on the number of operations required to solve the problem exceeds the number of operations required to solve the formulation presented in Sec. III.A by enumeration. Table 2 shows the upper bounds on the number of operations required to evaluate the costs and constraints associated with the MILP formulation if the problem had to be solved by enumeration. In practice, a MILP solver using branch and bound methods will solve such problems using fewer operations; however, in the worst case, the solver may have to evaluate the costs and constraints associated with all combinations of control inputs. The bounds provided here may be used to calculate the computation time required to solve the MILP problem by enumeration for any selected processor, compiler, and level of floating point. The resulting operation counts can be used to determine the worst-case computation time required to solve the problem for any selected processor, compiler, and level of numerical precision. Uncertainty in the time required to solve the MILP problem using optimization methods, such as branch and bound, may preclude the use of MILP in a real-time flight-critical application. The certainty and lower worst-case operation count, associated with using the enumeration method described in Sec. III.A, may make it more attractive than the MILP formulation for real-time operation. Nevertheless, in the examples that follow, the MILP formulation was used and solved using a compiled version of the GNU Linear Programming Kit (GLPK) within a MATLAB/Simulink environment.

D. Parameter Tuning

Recall that the primary objective is to minimize the quantization errors without exceeding the magnitude of the continuous torque commands in each axis. The secondary objective is to minimize the number of jets that are used at any given time in an effort to minimize propellant usage. Thus $w_1, \ldots, w_p \ll w_{\text{roll}}, w_{\text{pitch}}, w_{\text{yaw}}$, and it has been found that $w_k = 0.01, \forall\ k = 1, \ldots, p$, and roll, pitch, and yaw weights on the order of one yield acceptable results in the case studies presented in this paper. It has also been found that, when the norm of the tracking error is large, dynamically adjusting the axis weights based on the instantaneous values of the tracking errors in each axis can improve closed-loop attitude tracking responses when using the MILP RCS allocation scheme. In particular,

$$w_{\text{axis}_i} = \max\left(\frac{e_{\text{axis}_i}}{\|\mathbf{e}_{\text{axis}}\|_2}, 0.1\right) \tag{9}$$

where $\mathbf{e}_{\text{axis}}$ is a vector whose elements represent the tracking errors in each axis. Although such an approach improves tracking performance, the quantizer is no longer static. When the norm of the tracking error vector approaches zero, it was found that terminal limit cycle amplitudes were reduced by using equal weights on each axis. The threshold for turning dynamic axis weighting on or off is problem-dependent and should be tuned by the designer for best performance.

A note on the quantization constraint of Eq. (4) is also in order. Although it is intuitively appealing to preserve the sign of the continuous torque command in each axis, our studies have shown that imposing the sign constraint can lead to degraded tracking performance. When the sign constraint is violated, the sign of the feedback loop is effectively changed, which can lead to destabilizing behavior in the short term. In the long term, however, it may sometimes be advantageous to allow a short-term decrease in tracking performance to occur in one axis to improve performance in the other two, and correct for the buildup in tracking error in the first axis later. Thus, relaxing the sign constraint (i.e., the left-hand side) of Eq. (4) can significantly improve tracking performance for certain systems.

IV. Examples

A. Exoatmospheric Flight

For the purpose of demonstrating the method, we present some exoatmospheric results on a representative model of a reusable launch vehicle. We assume that the vehicle is equipped with 10 ideal thrusters that produce 800 lbf of thrust each. The inertia tensor (in a body-axis coordinate frame) for the vehicle is given by

$$\mathbf{J} = \begin{bmatrix} 433,000 & 0 & 0 \\ 0 & 960,000 & 0 \\ 0 & 0 & 1,130,000 \end{bmatrix} \text{ft}^2 \cdot \text{slug} \tag{10}$$

The torque matrix whose elements represent the firing torque produced by each thruster is assumed to be constant and is given by

$$\mathbf{T} = \begin{bmatrix} 0 & -1511 & 8574 & -5098 & 0 & 1515 & -8573 & 5098 & 0 & 0 \\ -367 & 0 & -6982 & 8702 & -367 & 0 & -6981 & 8702 & -367 & -367 \\ 14,675 & -11,597 & -6981 & -8702 & -14,675 & 11,597 & 6981 & 8702 & -14,675 & 14,675 \end{bmatrix} \text{ft} - \text{lbf} \tag{11}$$

The equations of motion are given by

$$\boldsymbol{\tau} = \mathbf{J}\dot{\boldsymbol{\omega}} \tag{12}$$

where $\boldsymbol{\tau} \in \mathbb{R}^3$ is a vector whose elements are the sum of all external torques applied to the vehicle, and $\boldsymbol{\omega} \in \mathbb{R}^3$ is a vector whose elements represent the roll rate p, pitch rate q, and yaw rate r. The Euler angle rate equations are given by

$$\dot{\phi} = p + \sin(\phi)\tan(\theta)q + \cos(\phi)\tan(\theta)r \tag{13}$$

$$\dot{\theta} = \cos(\phi)q - \sin(\phi)r \tag{14}$$

$$\dot{\psi} = \sin(\phi)\sec(\theta)q + \cos(\phi)\sec(\theta)r \tag{15}$$

For the purposes of this demonstration, we make use of a small angle approximation where

$$\dot{\phi} \approx p, \qquad \dot{\theta} \approx q, \qquad \dot{\psi} \approx r \tag{16}$$

Solving Eq. (12) for $\dot{\boldsymbol{\omega}}$ and making use of the small angle approximation of Eq. (16), we can produce a linear model of the system in state-space form:

$$\dot{\mathbf{x}} = \mathbf{A}\mathbf{x} + \mathbf{B}\boldsymbol{\tau} \qquad \mathbf{y} = \mathbf{C}\mathbf{x} \tag{17}$$

where $\mathbf{x} \triangleq [p, \phi, q, \theta, r, \psi]^T$, $\boldsymbol{\tau} \triangleq [\tau_{\text{roll}}, \tau_{\text{pitch}}, \tau_{\text{yaw}}]^T$, and

Table 2 Upper bounds on number of operations required at each flight control system update to solve quantized control allocation problem using MILP formulation

Operation	Number
Multiplications	$3(2^p)$
Multiplications by 0 or 1	$13(2^p)$
Additions	$(13p-7)(2^p)$
Comparisons	$18(2^p)$

$$\mathbf{A}=\begin{bmatrix}0&0&0&0&0&0\\1&0&0&0&0&0\\0&0&0&0&0&0\\0&0&1&0&0&0\\0&0&0&0&0&0\\0&0&0&0&1&0\end{bmatrix},\quad \mathbf{B}=\begin{bmatrix}I_{xx}^{-1}&0&0\\0&0&0\\0&I_{yy}^{-1}&0\\0&0&0\\0&0&I_{zz}^{-1}\\0&0&0\end{bmatrix}$$
$$\mathbf{C}=\begin{bmatrix}0&1&0&0&0&0\\0&0&0&1&0&0\\0&0&0&0&0&1\end{bmatrix} \tag{18}$$

Note that the vehicle dynamics are a bank of decoupled integrators; however, as can be inferred from Eq. (11), the RCS jets introduce a great deal of coupling between the axes when fired.

A continuous state feedback tracking control law is designed to produce a decoupled bank of second-order systems of the form

$$y_i=\frac{\omega_n^2}{s^2+2\zeta\omega_n s+\omega_n^2}y_{i_{\text{ref}}} \tag{19}$$

where $\zeta=0.7$ and $\omega_n=3$ rad/s. If the control effectors were capable of producing any specified value of torque, the following control law would produce the desired results:

$$\boldsymbol{\tau}=-\mathbf{J}\begin{bmatrix}2\zeta\omega_n&\omega_n^2&0&0&0&0\\0&0&2\zeta\omega_n&\omega_n^2&0&0\\0&0&0&0&2\zeta\omega_n&\omega_n^2\end{bmatrix}\mathbf{x}+\mathbf{J}\begin{bmatrix}\omega_n^2&0&0\\0&\omega_n^2&0\\0&0&\omega_n^2\end{bmatrix}\begin{bmatrix}\phi_{\text{ref}}\\\theta_{\text{ref}}\\\psi_{\text{ref}}\end{bmatrix} \tag{20}$$

or, in a more compact form,

$$\boldsymbol{\tau}_{\text{des}}=-\mathbf{K}\mathbf{x}+\mathbf{R}\mathbf{y}_{\text{ref}} \tag{21}$$

Because we are using 10 RCS thrusters that have two states each, there are $2^{10}=1024$ possible combinations of thruster firings that can be used to approximate the torque command generated by the tracking control law. As discussed previously, the MILP-based control allocator is formulated to determine the firing solution that most closely approximates the torque vector generated by the continuous control law, without exceeding the continuous torque command in any axis. A block diagram of the control system structure is shown in Fig. 5. Note that the MILP control allocator acts as a nonuniform multi-input/multi-output quantizer.

Figure 6 shows an initial condition response of the roll, pitch, and yaw angles using the RCS effectors when driven by the MILP control allocator. If a suite of continuously variable unlimited control effectors were available, each response would appear to be that of a second-order transfer function with a natural frequency of 3 rad/s and 0.7 damping ratio. Because the MILP allocator attempts to implement the continuous control law using RCS thrusters, which limit the torque resolution, we see that the responses generally exhibit the characteristics of a system with less damping. Eventually the responses settle into a low-amplitude limit cycle about zero error. Figure 7 shows the desired and quantized values of torque achieved in the roll, pitch, and yaw axes, respectively. One can see that control saturation is a predominant feature in these time histories. One can also see that the magnitude of the torques produced by the RCS system is always less than or equal to the torque command, which is a consequence of our choice of quantization method. It can also be seen that the sign of the RCS torque may be the opposite of the command in some cases, which, as noted previously, seems counterintuitive. However, as discussed in the section on parameter tuning, it is sometimes advantageous to allow a short-term decrease in tracking performance in one axis to improve performance in the other two, and to correct for the buildup in tracking error in the first axis later. In this case, relaxing the sign constraint (i.e., the left-hand side) of Eq. (4) significantly improved tracking performance for this system.

We now consider a failure case where jet numbers 3 and 7 become inoperable. Assuming that an FDI system is in place to identify the failure, elements in columns 3 and 7 of the torque matrix T, given in Eq. (11), are set to zero and the control allocation problem is solved using the modified torque matrix. Figure 8 shows an initial condition response for the vehicle attitude for the previously described failure case. By comparing the failed attitude response to the nominal response shown in Fig. 6, one can see that the settling time is increased and that the tracking performance degrades; however, the system ultimately regulates the attitude to near zero values in a low-amplitude terminal limit cycle. This example illustrates the potential of the method for use as an element of a reconfigurable flight control system that could be used to expand the capabilities of integrated adaptive guidance and control methods that have been specifically designed for endoatmospheric flight [14], where a combination of RCS and aerodynamic control surfaces are available.

B. Comparison of Mixed-Integer Linear Programming Reaction Control Systems Allocator to Pulse Width Modulation

The MILP RCS allocation algorithm was designed to minimize both propellant usage and jet cycling. An alternative approach to control allocation of RCS jets that is appropriate for multi-axis coupled systems is that proposed by Paradiso [6]. Paradiso proposed treating RCS jets as continuously variable control effectors for the purpose of formulating an LP-based control allocation problem with continuous variables. The continuous outputs for the jets were interpreted as duty cycle commands for a pulse width modulation scheme, wherein the jets were cycled on/off over a fixed period of time (short when compared to the bandwidth of the system dynamics) to produce a time-averaged moment that approximated

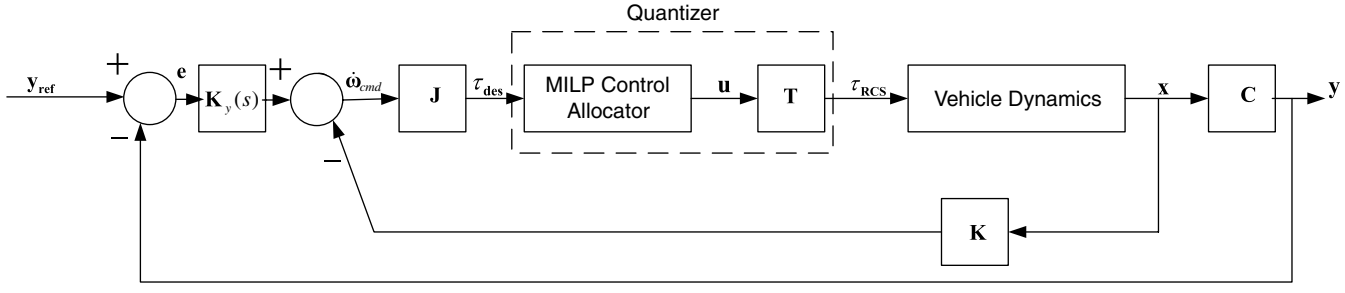

Fig. 5 Block diagram of attitude tracker using MILP control allocator for RCS firing logic for exoatmospheric flight.

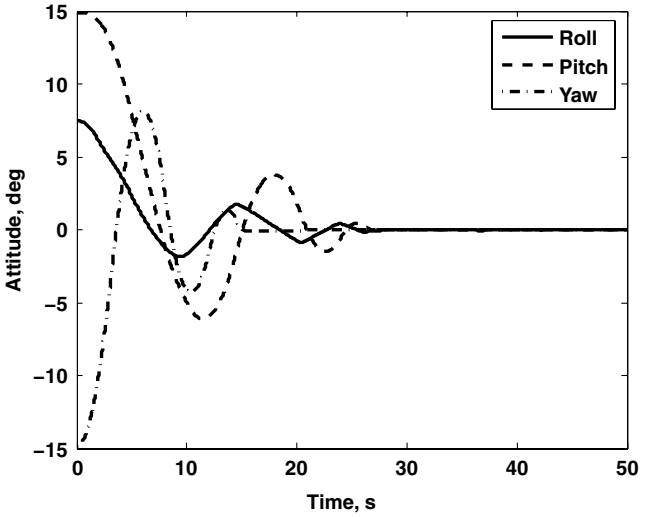

Fig. 6 Exoatmospheric initial condition response with MILP control allocator.

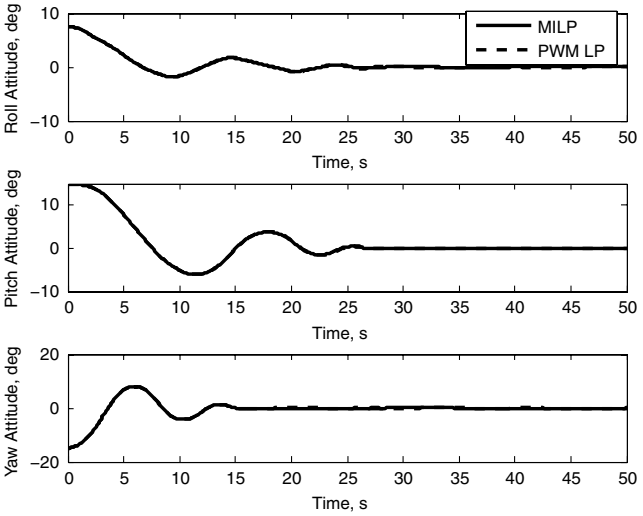

Fig. 9 Comparison of closed-loop responses using MILP and LP-based PWM control allocators.

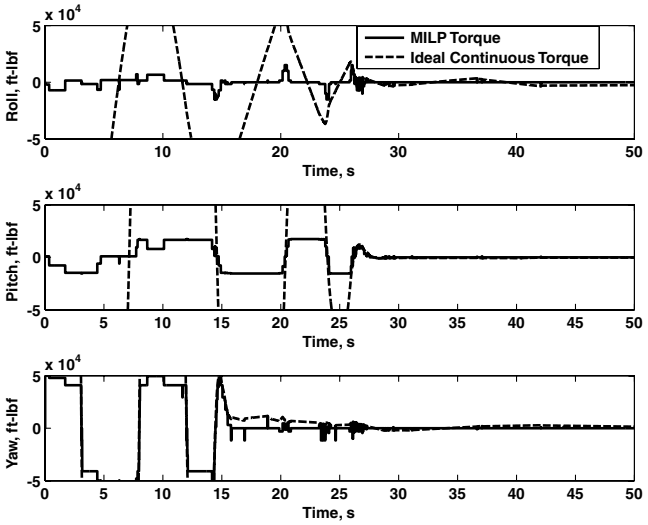

Fig. 7 Comparison of exoatmospheric continuous feedback controller torque commands and MILP RCS torques.

the desired moment. The MILP algorithm developed in this paper will now be compared with an LP-based PWM approach.

A linear programming formulation of the exoatmospheric control allocation problem was constructed exactly as described in Eq. (8), *except* the decision variables were not restricted to be binary, but were treated as real numbers between zero and one, inclusive. The decision variable solutions are duty cycle commands that are processed by a PWM module that provided on/off commands to each jet.

The example considered here is a case where the cycle-time granularity of the jets is less than the flight control system sample rate. The MILP algorithm results in the previous section were generated from a simulation and flight control system that ran at a fixed time step of 20 ms. For the purposes of comparing the MILP to an LP PWM approach, the simulation ran at a fixed time step of 4 ms, while the flight control system sampled the dynamic system outputs every 20 ms. The pulse width modulator processed the output of the LP control allocator, which consisted of a vector of duty cycle commands for each of the 10 jets and generated on/off commands to each thruster of durations that were integer multiples of 4 ms, with a maximum of one transition from on/off per 20 ms. The duty cycle commands are therefore rounded to the nearest 20% of the 20 ms flight control command update period, resulting in possible pulse duration periods of 0, 4, 8, 12, 16, and 20 ms. Thus, the cycle-time

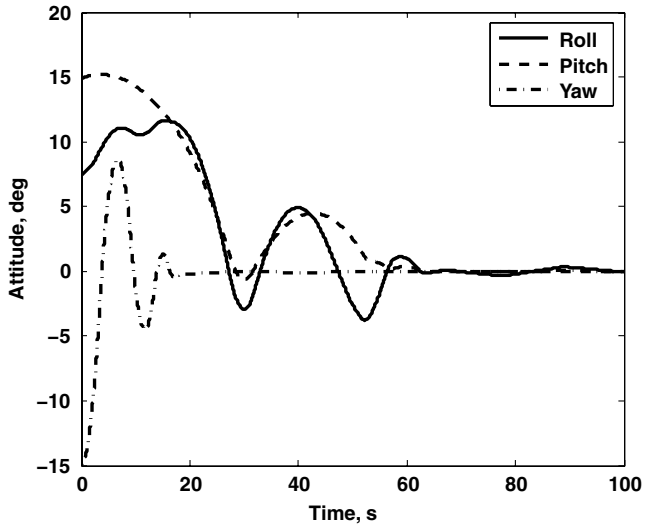

Fig. 8 Initial condition response with MILP control allocator for jet numbers 3 and 7 failed off.

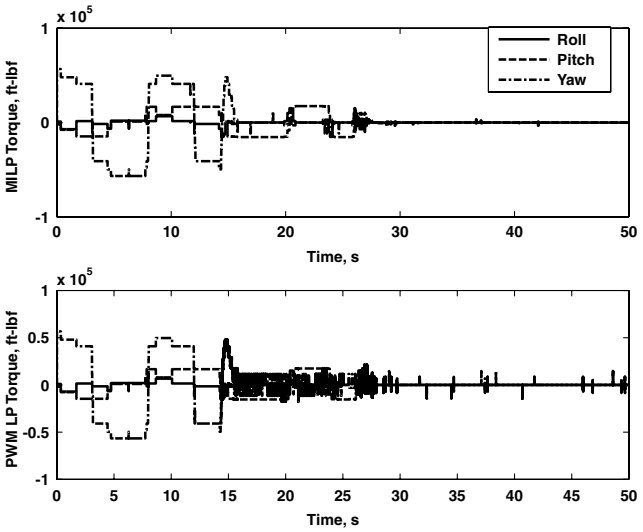

Fig. 10 Comparison of net torque commands from MILP and PWM LP control allocators.

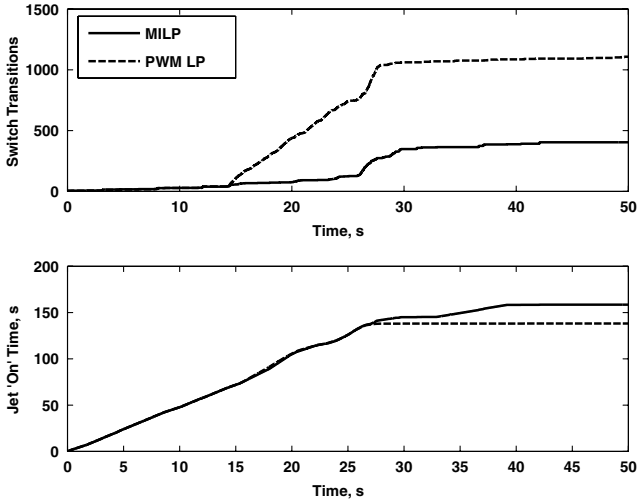

Fig. 11 Comparison of switching behavior and propellant usage of MILP and PWM LP control allocators.

granularity for the hypothetical jets considered in this comparison is 4 ms.

Figure 9 compares an initial condition response of attitude time histories of the vehicle when operating under MILP and LP-based PWM-driven RCS jets. For the initial condition response, the controller acts as a regulator, thus, attitude and attitude error are synonymous in the plot. It can be seen that there is very little difference between the closed-loop behavior of the system operating under MILP quantized control vs LP-based PWM control.

Figure 10 shows the pitch, roll, and yaw torques applied by the PWM and MILP allocators. As expected, the LP-based PWM switches more often than the MILP approach. Figure 11 shows the switch cycle time history. It can be seen that the switch cycles grow at nearly the same rate in the transient, however, the switching behavior of the PWM LP algorithm increases as the response goes toward zero. The MILP approach results in 404 switch cycles, whereas the PWM results in 1108. Thus, the PWM cycles the jets 2.74 times as often as the MILP.

In spite of the fact that the PWM cycles more often, it uses less propellant. Figure 11 shows the propellant usage as a function of time for each approach. Both approaches use comparable amounts of propellant in the transient phase; however, the PWM uses far less propellant in the terminal limit cycle phase. This occurs for two reasons: one is that the PWM is capable of producing thrust pulses of shorter duration and thus can make corrections that use less propellant, and the second is that, because of the shorter pulse duration, finer tracking can be achieved because the PWM has higher effective torque resolution which enables it to more closely approximate the linear control command. This property leads to lower terminal limit cycle amplitudes that require less propellant to correct. It is worth noting that the switch count of the PWM approach is heavily influenced by the resolution of the duty cycle of the PWM. The solution to the MILP formulation is similar to a limiting case where the PWM has only two choices for duty cycle, 0 and 100%. If the LP approach were used to solve for the duty cycle, the results would be rounded to 0 or 100%. The resulting LP and rounding function would therefore provide a relaxed solution to the MILP.

C. Endoatmospheric Flight

Figure 12 shows a block diagram of a control allocator structure for use in endoatmospheric flight. In this case, the aerodynamic surfaces are driven by a continuous allocator to achieve the desired moment commanded by the control law. In the event that the desired moment is unattainable using aerodynamic surfaces alone, the MILP RCS allocator is used to determine an RCS firing solution to reduce the torque residual without exceeding the total torque command. The MILP allocator is therefore daisy-chained with a continuous control allocator, and quantization occurs only when the torque command in any given axis lies outside of the attainable moment set associated with the aerodynamic surfaces. Implementation of the MILP allocator alone generally results in limit cycle behavior about the origin in error and error rate space; however, when used in conjunction with a continuous allocator when aerodynamic surface control power is available, the error trajectories can be driven to the origin.

In the following example, a discrete MILP RCS control allocator is combined with an LP-based continuous control allocator that mixes the aerodynamic control effectors in a simulation of a representative reusable launch vehicle. The baseline vehicle is longitudinally unstable at Mach numbers above five during descent and directionally unstable at all Mach numbers. The vehicle is laterally stable at all Mach numbers. The simulation uses full 6-degree-of-freedom equations of motion, a dynamic inversion based reconfigurable control law, and an atmospheric model. The RCS MILP was then added to the simulation to augment the control power from the aerodynamic control surfaces to more closely approximate the torque vector commanded by the dynamic inversion control law. In effect, when the aerodynamic surfaces saturate or are unable to provide the required moments to maintain tracking or to recover from disturbances, the RCS is activated to assist, provided that doing so does not cause any element of the torque vector to exceed the values commanded by the dynamic inversion control law.

To demonstrate the functionality of the model, initial trim conditions are found at 190,000 ft during descent and a failure condition is applied. The left flap, which normally provides a substantial amount of yaw attitude control, is fixed at 0 deg for this example. Because the aircraft is unstable in yaw, this type of control failure would have severe consequences if compensation were not applied. The simulation is run both with and without the assistance of

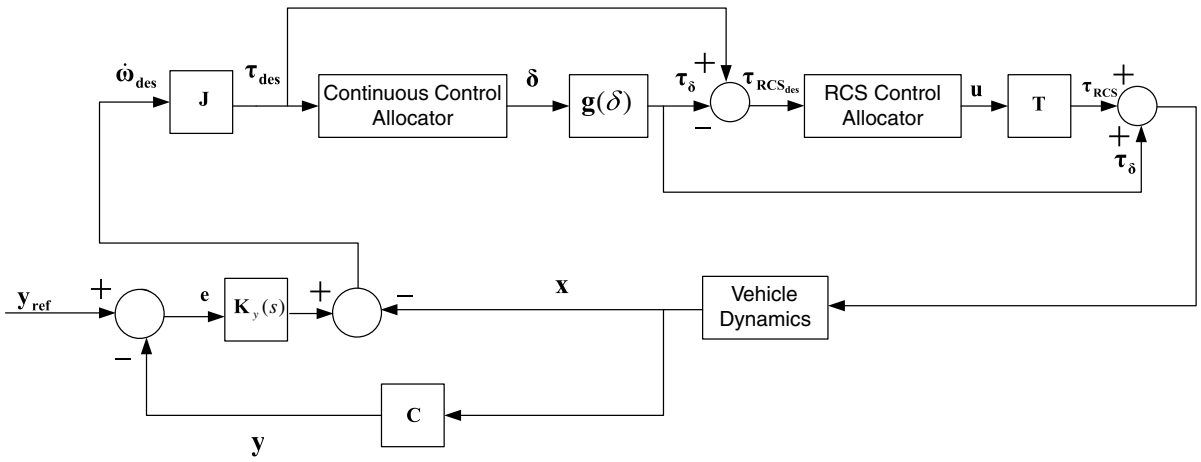

Fig. 12 Block diagram of attitude tracker using daisy-chained continuous and RCS control allocators for endoatmospheric flight.

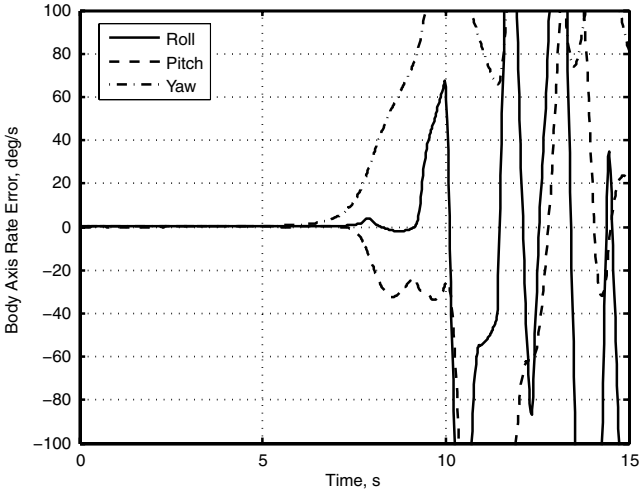

Fig. 13 Tracking error with left flap fixed (no RCS).

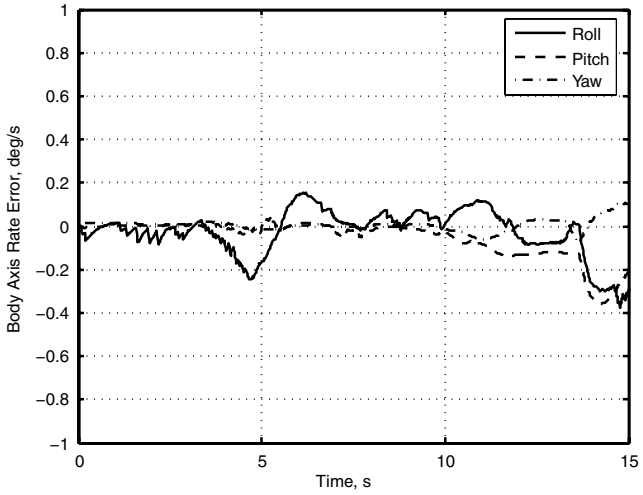

Fig. 14 Tracking error with left flap fixed (with RCS).

the MILP RCS system. Figure 13 shows the tracking error without the assistance of the RCS. The aerodynamic control surfaces possess enough authority to keep the vehicle tracking for about 8 s. However, as dynamic pressure increases, the working control surfaces cannot overcome the fixed flap and they saturate, causing the vehicle to go unstable. When the simulation is run with the RCS activated, the results are much more favorable. Figure 14 shows the tracking results with the RCS and aerodynamic surfaces blended together.

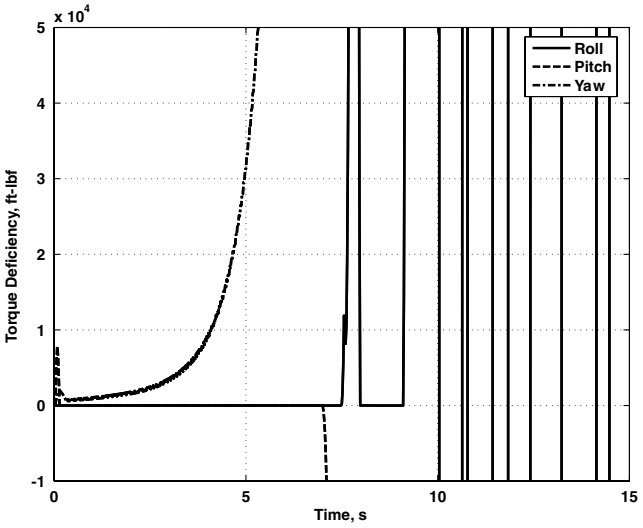

Fig. 15 Torque error with left flap fixed (no RCS).

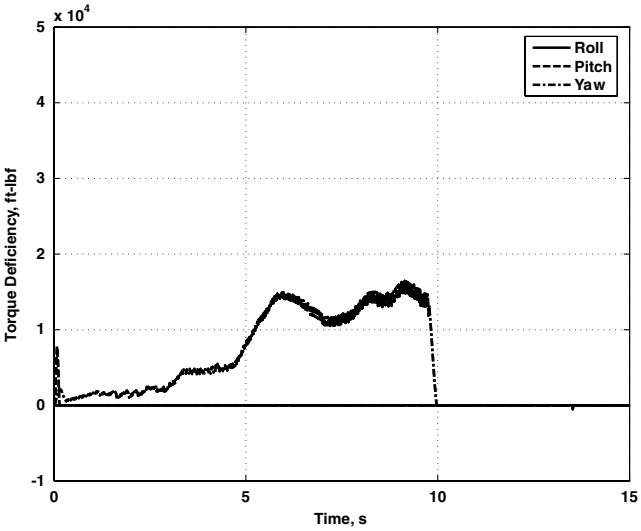

Fig. 16 Torque error with left flap fixed (with RCS).

Figure 15 shows the difference in torque required and torque applied by the aerosurfaces with no RCS engaged. Just before the 8 s point, the torque error increases rapidly and the aerosurfaces are unable to provide the necessary moments, causing the vehicle to quickly go unstable. The addition of the RCS allows the vehicle to maintain stable flight over the 15 s simulation run. Figure 16 shows the error in torque with both the aerosurfaces and RCS providing the necessary moments to the vehicle. The blending of two types of control effectors keeps the errors relatively small. Errors still exist due to the nature of the quantized controller, but the combined system performs fairly well. Note also that the addition of the RCS primarily keeps the torque errors positive. The RCS logic is designed to never overtorque the aircraft, which is expected because the quantized controller is designed to avoid overtorquing the vehicle.

V. Guaranteed Stability Under Quantized State Feedback

The closed-loop stability of continuous systems, operating under the influence of continuously variable control inputs, has been well studied, and an enormous variety of multivariable control synthesis methodologies exist to solve such problems. The philosophy of using a quantized control allocation method, as presented here, is to allow one to make use of well-established control design methods for continuously variable control effectors, for systems where the control inputs must be chosen from a finite set of distinct inputs. As stated in the Introduction, phase-plane methods have been the traditional tool of choice for designing control laws for distinct input systems where multi-axis coupling is weak; however, when multi-axis coupling is strong, such methods become cumbersome control synthesis tools. In the present case, RCS jets are only capable of producing a finite number of distinct torques, and it is of interest to determine how the stabilization properties of a continuous control law are altered by the implementation of a quantized approximation of the control law that makes use of pulsed control effectors.

The impact of quantization on closed-loop vehicle stability will be addressed. To make the discussion precise, we make use of the following definitions. Given a vector $\mathbf{x} \in \mathbb{R}^n$, the standard Euclidean norm $\|\mathbf{x}\|$ is

$$\|\mathbf{x}\| = \sqrt{\sum_{i=1}^{n} x_i^2}$$

It is also useful to note the following inequality:

$$\|\mathbf{x}\| \leq \sqrt{n}\|\mathbf{x}\|$$

The quantization function $q(x)$ is defined by

$$q(u) = \begin{cases} M & \text{if } u > M \\ \max\{k \in \Delta \cdot \mathbb{Z}\colon k \le u\} & \text{if } -M < u < M \\ -M & \text{if } u \le M \end{cases}$$

with $\mathbb{Z}$ being the set of nonnegative integers, $M > 0$ being the actuator saturation level, and Δ being a quantization increment.

Given a state feedback regulation problem for a linear, continuous time-invariant system

$$\mathbb{S} = \begin{cases} \dot{\mathbf{x}} = \mathbf{A}\mathbf{x} + \mathbf{B}\mathbf{u} \\ \mathbf{x}(0) = \mathbf{x}_0 \end{cases} \tag{22}$$

where $\mathbf{x} \in \mathbb{R}^n$, $\mathbf{u} \in \mathbb{R}^m$, $\mathbf{A} \in \mathbb{R}^{n\times n}$, and $\mathbf{B} \in \mathbb{R}^{n\times m}$. If a linear system as described in Eq. (22) is controllable, then there exists a matrix $\mathbf{K}$ such that all eigenvalues of $(\mathbf{A} - \mathbf{B}\mathbf{K})$ have negative real parts, that is, $\lambda(\mathbf{A} - \mathbf{B}\mathbf{K}) < \mathbf{0}$. In the following discussion, we will consider the domain of attraction in which the state feedback control signal $\mathbf{u} = -\mathbf{K}\mathbf{x}$ is quantized by the quantization function $\mathbf{q}(\cdot)$ such that

$$\mathbf{u}_q = \mathbf{q}(\mathbf{u}) = \mathbf{q}(-\mathbf{K}\mathbf{x})$$

Consider the following

$$\begin{cases} \dot{\mathbf{x}} & = \mathbf{A}\mathbf{x} + \mathbf{B}\mathbf{u}_q \\ \mathbf{u}_q & = \mathbf{q}(-\mathbf{K}\mathbf{x}) \end{cases} \tag{23}$$

or

$$\dot{\mathbf{x}} = \mathbf{A}\mathbf{x} + \mathbf{B}\mathbf{q}(-\mathbf{K}\mathbf{x}) = \mathbf{A}\mathbf{x} + \mathbf{B}(-\mathbf{K}\mathbf{x}) + \mathbf{B}\mathbf{q}(-\mathbf{K}\mathbf{x}) - \mathbf{B}(-\mathbf{K}\mathbf{x}) = (\mathbf{A} - \mathbf{B}\mathbf{K})\mathbf{x} + \mathbf{B}\underbrace{[\mathbf{q}(-\mathbf{K}\mathbf{x}) + \mathbf{K}\mathbf{x}]}_{\text{diff. due to quant.}} \tag{24}$$

Let $\mathbf{e} = \mathbf{q}(-\mathbf{K}\mathbf{x}) + \mathbf{K}\mathbf{x}$ be the error in the full-state feedback control signal $\mathbf{K}\mathbf{x}$ caused by the quantization process $\mathbf{q}(-\mathbf{K}\mathbf{x})$. From Eq. (24), we have

$$\begin{cases} \dot{\mathbf{x}} = (\mathbf{A} - \mathbf{B}\mathbf{K})\mathbf{x} + \mathbf{B}\mathbf{e} \\ \mathbf{e} = \mathbf{q}(-\mathbf{K}\mathbf{x}) + \mathbf{K}\mathbf{x} \end{cases} \tag{25}$$

From Lyapunov stability theory, it is well known that there exists a symmetric, positive definite matrix $\mathbf{P}$, that is, $\mathbf{P} > \mathbf{0}$, such that

$$(\mathbf{A} - \mathbf{B}\mathbf{K})^T\mathbf{P} + \mathbf{P}(\mathbf{A} - \mathbf{B}\mathbf{K}) = -\mathbf{Q} \tag{26}$$

if $(\mathbf{A} - \mathbf{B}\mathbf{K})$ is stable, that is, real$[\lambda(\mathbf{A} - \mathbf{B}\mathbf{K})] < \mathbf{0}$, and $\mathbf{Q}$ is symmetric, positive definite, that is, $\mathbf{Q} > \mathbf{0}$. Because $\mathbf{P} > \mathbf{0}$, the scalar function $V = \mathbf{x}^T\mathbf{P}\mathbf{x}$ is positive for any $\mathbf{x}$. Thus, we can choose $V = V(\mathbf{x})$ to be a Lyapunov function for the system described in Eq. (25), and examine the condition under which the system is asymptotically stable, that is, its time-derivative is negative: $(\mathrm{d}/\mathrm{d}t)(\mathbf{x}^T\mathbf{P}\mathbf{x}) < 0$:

$$(\mathrm{d}/\mathrm{d}t)V = (\mathrm{d}/\mathrm{d}t)(\mathbf{x}^T\mathbf{P}\mathbf{x}) = \dot{\mathbf{x}}^T\mathbf{P}\mathbf{x} + \mathbf{x}^T\mathbf{P}\dot{\mathbf{x}} \tag{27}$$

Substituting $\dot{\mathbf{x}}$ in Eq. (25) into Eq. (27), we have

$$\dot{V} = \dot{\mathbf{x}}^T\mathbf{P}\mathbf{x} + \mathbf{x}^T\mathbf{P}\dot{\mathbf{x}} = [\mathbf{x}^T(\mathbf{A} - \mathbf{B}\mathbf{K})^T + \mathbf{e}^T\mathbf{B}^T]\mathbf{P}\mathbf{x} + \mathbf{x}^T\mathbf{P}[(\mathbf{A} - \mathbf{B}\mathbf{K})\mathbf{x} + \mathbf{B}\mathbf{e}] = \mathbf{x}^T[(\mathbf{A} - \mathbf{B}\mathbf{K})^T\mathbf{P} + \mathbf{P}(\mathbf{A} - \mathbf{B}\mathbf{K})]\mathbf{x} + 2\mathbf{x}^T\mathbf{P}\mathbf{B}\mathbf{e} \tag{28}$$

Combining Eqs. (26) and (28), we have

$$\dot{V} = \underbrace{-\mathbf{x}^T\mathbf{Q}\mathbf{x}}_{\text{negative}} + \underbrace{2\mathbf{x}^T\mathbf{P}\mathbf{B}\mathbf{e}}_{\text{undertermined}} \tag{29}$$

In Eq. (29), the first term $(-\mathbf{x}^T\mathbf{Q}\mathbf{x})$ is always negative because $\mathbf{Q}$ is positive definite. The second term $(2\mathbf{x}^T\mathbf{P}\mathbf{B}\mathbf{e})$ is undetermined. Thus, a *sufficient* condition for $\dot{V}$ to be negative, that is, the system $\mathbb{S}$ in Eq. (23) is stable under the quantized state feedback $\mathbf{u}_q = \mathbf{q}(-\mathbf{K}\mathbf{x})$, is

$$\|2\mathbf{x}^T\mathbf{P}\mathbf{B}\mathbf{e}\| < \|\mathbf{x}^T\mathbf{Q}\mathbf{x}\| \tag{30}$$

Also, we will make use of the following bounds

$$\|\mathbf{x}\|^2\sigma_{\min}(\mathbf{Q}) \le \|\mathbf{x}^T\mathbf{Q}\mathbf{x}\| \tag{31}$$

and

$$\|2\mathbf{x}^T\mathbf{P}\mathbf{B}\mathbf{e}\| \le 2\|\mathbf{x}\|\sigma_{\max}(\mathbf{P})\sigma_{\max}(\mathbf{B})\|\mathbf{e}\| \tag{32}$$

where $\sigma_{\min}(\,)$ and $\sigma_{\max}(\,)$ represent the minimum and maximum singular values of their matrix argument. Thus inequality (30) is satisfied if

$$2\|\mathbf{x}\|\sigma_{\max}(\mathbf{P})\sigma_{\max}(\mathbf{B})\|\mathbf{e}\| \le \|\mathbf{x}\|^2\sigma_{\min}(\mathbf{Q})$$

or

$$\|\mathbf{x}\| \ge \frac{2\sigma_{\max}(\mathbf{P})\sigma_{\max}(\mathbf{B})\|\mathbf{e}\|}{\sigma_{\min}(\mathbf{Q})} \tag{33}$$

At this point, we note that

$$\|\mathbf{e}\| = \|\mathbf{q}(-\mathbf{K}\mathbf{x}) + \mathbf{K}\mathbf{x}\| \le \Delta\sqrt{n} \tag{34}$$

Combining inequalities (33) and (34), we have

$$\|\mathbf{x}\| \ge \frac{2\sigma_{\max}(\mathbf{P})\sigma_{\max}(\mathbf{B})\Delta\sqrt{n}}{\sigma_{\min}(\mathbf{Q})}$$

where Δ is the quantization length and n is the order of the plant model. In summary, the preceding discussion contains the following implication. For the system described in Eq. (25), we can choose Lyapunov function $V = \mathbf{x}^T\mathbf{P}\mathbf{x} > 0$ so that

$$\mathbf{x} \in \mathbb{L} = \left\{\mathbf{x}\colon \|\mathbf{x}\| \ge \frac{2\sigma_{\max}(\mathbf{P})\sigma_{\max}(\mathbf{B})\Delta\sqrt{n}}{\sigma_{\min}(\mathbf{Q})}\right\} \Rightarrow \dot{V} < 0 \tag{35}$$

Consequently, the system $\mathbb{S}$ in Eq. (23) is stable under the quantized state feedback $\mathbf{u}_q = \mathbf{q}(-\mathbf{K}\mathbf{x})$ if $\mathbf{x}(\mathbf{0}) = \mathbf{x}_\mathbf{0} \in \mathbb{L}$. The state-space region $\mathbb{L}$ shown in Eq. (35) defines the *domain of attraction*. Equation (35) also shows the impact that the quantization length Δ has on this region $\mathbb{L}$.

In the following discussion, we will apply the preceding results to the example in Sec. IV.A. The given plant has 10 thrusters that can be used to actuate the vehicle about the vehicle-axis torque space τ_x, τ_x, τ_z. Within any actuation time interval, there exists $2^{10} = 1024$ possible combinations from which an optimal choice can be made. Furthermore, the quantization length Δ may vary from axis to axis and is not known a priori under the proposed MILP RCS allocation scheme. It is then useful to explore a way to quantify a guaranteed region of attraction under a nonuniform, but finite, dimension quantization for a given initial condition $\mathbf{x}(\mathbf{t}_\mathbf{o})$. We propose a method to specify a priori a guaranteed region of attraction by examining how the worst-case $e(t)$ impacts a guaranteed region of attraction. Given Eq. (25) and the state vector at $t = t_o$, we calculate the maximum magnitude of the control input error $|\mathbf{e}| = |\mathbf{q}(-\mathbf{K}\mathbf{x}) + \mathbf{K}\mathbf{x}|$. This maximum magnitude $|\mathbf{e}_{\max}(\mathbf{t})| = \bar{e}$ can then be used to provide the bound of a region of attraction $\mathbb{L}$ for $\mathbf{x}(\mathbf{t})$, as shown in Eqs. (33) and (35). For the current example, with

$$\mathbf{x}(t) = \begin{bmatrix} p(t) \\ \phi(t) \\ q(t) \\ \theta(t) \\ r(t) \\ \psi(t) \end{bmatrix}, \qquad \mathbf{x}(t_o) = \begin{bmatrix} 0.00 \\ 0.13 \\ 0.00 \\ 0.26 \\ 0.00 \\ -0.26 \end{bmatrix}$$

$$\mathbf{A} = \begin{bmatrix} 0 & 0 & 0 & 0 & 0 & 0 \\ 1 & 0 & 0 & 0 & 0 & 0 \\ 0 & 0 & 0 & 0 & 0 & 0 \\ 0 & 0 & 1 & 0 & 0 & 0 \\ 0 & 0 & 0 & 0 & 0 & 0 \\ 0 & 0 & 0 & 0 & 1 & 0 \end{bmatrix}$$

$$\mathbf{B} = \begin{bmatrix} I_{xx}^{-1} & 0 & 0 \\ 0 & 0 & 0 \\ 0 & I_{yy}^{-1} & 0 \\ 0 & 0 & 0 \\ 0 & 0 & I_{zz}^{-1} \\ 0 & 0 & 0 \end{bmatrix} = \begin{bmatrix} 0.2309 & 0 & 0 \\ 0 & 0 & 0 \\ 0 & 0.1042 & 0 \\ 0 & 0 & 0 \\ 0 & 0 & 0.0885 \\ 0 & 0 & 0 \end{bmatrix} \times 10^{-5}$$

we design the full-state feedback $\mathbf{K}$ to obtain the desired damping $\zeta = \sqrt{2}/2$ and oscillation $\omega_n = 3$ rad/s

$$\mathbf{K} = \begin{bmatrix} 1.8407 & 3.9053 & 0 & 0 & 0 & 0 \\ 0 & 0 & 4.0741 & 8.6438 & 0 & 0 \\ 0 & 0 & 0 & 0 & 4.7960 & 1.0175 \end{bmatrix} \times 10^{6}$$

Solving Eq. (26) with $\mathbf{Q} = I_{6\times 6}$, we have

$$\mathbf{P} = \begin{bmatrix} 1.1787 & -0.5000 & 0 & 0 & 0 & 0 \\ -0.5000 & 0.3666 & 0 & 0 & 0 & 0 \\ 0 & 0 & 1.1787 & -0.5000 & 0 & 0 \\ 0 & 0 & -0.5000 & 0.3666 & 0 & 0 \\ 0 & 0 & 0 & 0 & 1.1787 & -0.5000 \\ 0 & 0 & 0 & 0 & -0.5000 & 0.3666 \end{bmatrix}$$

and

$$\sigma_{\max}(\mathbf{P}) = 1.42$$
$$\sigma_{\max}(\mathbf{B}) = 0.23 \times 10^{-5}$$
$$\sigma_{\min}(\mathbf{Q}) = 1$$
$$\|\mathbf{e}_{\max}(\mathbf{t})\| = 3.46 \times 10^{6}$$

Thus, the bound shown in inequality (33) is negative for all $\mathbf{x}$ such that

$$\|\mathbf{x}\| \geq \frac{2\sigma_{\max}(\mathbf{P})\sigma_{\max}(\mathbf{B})\|\mathbf{e}\|}{\sigma_{\min}(\mathbf{Q})} = 22.63$$

Note that the guaranteed domain of attraction is defined by a region that lies *outside* of a ball centered at the origin in the state space. For state vectors lying outside of the ball, the trajectory is guaranteed to approach this ball. Because the stability criteria is based on sufficient conditions, no statements regarding the stability of trajectories inside of this ball may be made, they may be stable, unstable, or neutrally stable. Thus, the stability criteria is extremely conservative and its usefulness from a flight certification point of view may be limited. One can see that the time histories presented in Sec. IV.A converge to a low-amplitude limit cycle close to the origin, even though the norm of the initial state vector ($\|\mathbf{x}_o\| = 0.39$) lies in the region for which there is no guarantee of stability $\|\mathbf{x}\| < 22.63$. In the preceding example, the numerical results and the stability analysis were made with the given value of $\|\mathbf{x}_o\| = 0.39$. More often, in practical applications we are interested in a *region* $\mathbb{R}_i$ in the state space from which the initial state vector $\|\mathbf{x}_o\|$ evolves. We can extend the preceding discussion to cover such case. Because it has been shown that $V = \mathbf{x}^T\mathbf{P}\mathbf{x}$ is monotonically decreasing, $\|\mathbf{x}(t)\|$ will be less than $\|\mathbf{x}_o\|$ for all $t > 0$. We can use this fact to calculate $\|\mathbf{e}\|$ in Eq. (34) using only the values of $\|\mathbf{x}(t)\| \leq \|\mathbf{x}_o\|$. The computed values of $\|\mathbf{e}\|$ can be substituted into Eq. (36) to find a region of attraction $\mathbb{L}$ associated with $\mathbb{R}_i$:

$$\mathbf{x} \in \mathbb{L} = \left\{ \mathbf{x}\colon \|\mathbf{x}\| \geq \frac{2\sigma_{\max}(\mathbf{P})\sigma_{\max}(\mathbf{B})\|\mathbf{e}\|}{\sigma_{\min}(\mathbf{Q})} \right\} \tag{36}$$

VI. Conclusions

A mixed-integer linear programming formulation has been proposed for reaction control system control allocation for entry vehicles. An example with multi-axis control coupling was used to demonstrate that the method effectively blends the jets to approximate control torque vectors generated by a continuous control law under nominal and failed conditions. A structure has also been proposed that allows the MILP-based RCS control allocator to be used in conjunction with standard LP-based control allocators to augment saturated aerodynamic surfaces during the transition from exoatmospheric to endoatmospheric flight. The new method was compared with a linear-programming-based pulse width modulation scheme and was found to significantly reduce the number of RCS switch transitions. It was also found that the PWM approach consumed comparable amounts of propellent when rejecting transients; however, the PWM approach used significantly less propellant when operating in low-amplitude terminal attitude limit cycles than the MILP approach. A guaranteed domain of attraction for the quantized full-state feedback was derived using Lyapunov analysis. The results of the analysis were applied to the example to find the domain of attraction. The Lyapunov analysis revealed that the stability of the quantized RCS system can be guaranteed for an LTI system in a region located *outside* of a ball centered at the origin of the state space. When operating inside of the ball, no conclusive statements can be made about the stability of the system. The practical utility of the Lyapunov method for determining the region of attraction of a quantized control law was found to be limited due to the inherent conservatism of the method.

References

[1] Anon., "Guidance System Operations Plan for Manned CM Earth Orbital and Lunar Missions Using Program Colossus 3, Sec. 3, Digital Autopilots (Rev. 14)," NASA, Tech. Rept. MIT IL R-577, Contract NAS 9-4065, March 1972.

[2] Calhoun, P. C., and Queen, E. M., "Entry Vehicle Control System Design for the Mars Science Laboratory," *Journal of Spacecraft and Rockets*, Vol. 43, No. 2, 2006, pp. 324–329. doi:10.2514/1.19650

[3] Hattis, P. D., "Qualitative Differences Between Shuttle On-Orbit and Transition Control," *Journal of Guidance, Control, and Dynamics*, Vol. 7, No. 1, 1984, pp. 4–8. doi:10.2514/3.56361

[4] Alexander, N., Penchuk, P. D. H., and Kubiak, E. T., "Frequency Domain Stability Analysis of a Phase Plane Control System," *Journal of Guidance, Control, and Dynamics*, Vol. 8, No. 1, 1985, pp. 50–55. doi:10.2514/3.19934

[5] Muss, J., "Development of the X-33 gCH_4/gO_2 RCS Thruster," AIAA Paper 1999-2182, June 1999.

[6] Paradiso, J. A., "Adaptable Method of Managing Jets and Aerosurfaces for Aerospace Vehicle Control," *Journal of Guidance, Control, and Dynamics*, Vol. 14, No. 1, 1991, pp. 44–50. doi:10.2514/3.20603

[7] Bullo, F., and Liberzon, D., "Quantized Control via Locational Optimization," *IEEE Transactions on Automatic Control*, Vol. 51, No. 1, 2006, pp. 2–13. doi:10.1109/TAC.2005.861688

[8] Brockett, R. W., and Liberzon, D., "Quantized Feedback Stabilization of Linear Systems," *IEEE Transactions on Automatic Control*, Vol. 45, No. 7, 2000, pp. 1279–1289. doi:10.1109/9.867021

[9] Ishii, H., and Francis, B. A., "Stabilizing a Linear System by Switching Control with Dwell Time," *IEEE Transactions on Automatic Control*, Vol. 47, No. 12, 2002, pp. 1962–1973. doi:10.1109/TAC.2002.805689

[10] Bodson, M., "Evaluation of Optimization Methods for Control Allocation," *Journal of Guidance, Control, and Dynamics*, Vol. 25, No. 4, 2002, pp. 703–711.

[11] Enns, D., "Control Allocation Approaches," AIAA Paper 1998-4109, Aug. 1998, pp. 98–108.

[12] Bolender, M. A., and Doman, D. B., "Non-Linear Control Allocation Using Piecewise Linear Functions," *Journal of Guidance, Control, and Dynamics*, Vol. 27, No. 6, 2004, pp. 1017–1027. doi:10.2514/1.9546

[13] Oppenheimer, M. W., Doman, D. B., and Bolender, M. A., "Control Allocation for Overactuated Systems," *14th Mediterranean Conference on Control and Automation*, Inst. of Electrical and Electronics Engineers, MED 2006, June 2006.

[14] Schierman, J.,Ward, D., Hull, J., Gandhi, N., Oppenheimer, M., and Doman, D., "Integrated Adaptive Guidance and Control for Re-Entry Vehicles with Flight Test Results," *Journal of Guidance, Control, and Dynamics*, Vol. 27, No. 6, 2004, pp. 975–988. doi:10.2514/1.10344